CrossMark
click for updates

View Article Online
View Journal

Journal of
Materials Chemistry B

Accepted Manuscript

This article can be cited before page numbers have been issued, to do this please use: H. Wang, H. Wu, H. Shen, S. Geng, B. Wang, Y. Wang, X. Ma, G. Li and M. Tan, *J. Mater. Chem. B*, 2015, DOI: 10.1039/C5TB01160D.


This is an *Accepted Manuscript*, which has been through the Royal Society of Chemistry peer review process and has been accepted for publication.

*Accepted Manuscripts* are published online shortly after acceptance, before technical editing, formatting and proof reading. Using this free service, authors can make their results available to the community, in citable form, before we publish the edited article. We will replace this *Accepted Manuscript* with the edited and formatted *Advance Article* as soon as it is available.

You can find more information about *Accepted Manuscripts* in the Information for Authors.

Please note that technical editing may introduce minor changes to the text and/or graphics, which may alter content. The journal's standard Terms & Conditions and the Ethical guidelines still apply. In no event shall the Royal Society of Chemistry be held responsible for any errors or omissions in this *Accepted Manuscript* or any consequences arising from the use of any information it contains.

ROYAL SOCIETY OF CHEMISTRY

www.rsc.org/materialsB

View Article Online
DOI: 10.1039/C5TB01160D

Journal Name

ARTICLE

# A bimodal MRI and NIR liposome nanoprobe for tumor targeted molecular imaging

Received 00th January 20xx,
Accepted 00th January 20xx

DOI: 10.1039/x0xx00000x

www.rsc.org/

Huihui Wang[a,b §], Hao Wu[a,b §], Hujun Shen[d], Shaote Geng[a,c], Beibei Wang[a,b], Yanfang Wang[a,b], Xiaojun Ma[a], Guohui Li[d] and MingqianTan[a,c*]

The combination of complementary MRI and NIR imaging methods evolved to provide an even more powerful bioimaging tool. Herein, a novel bimodal MRI/NIR nanoprobe GCF-HDA was prepared via a facile self-assembly approach of three types of amphiphilic structures in aqueous solution. The Stokes shift of NIR moiety increased from 30 to 150 nm and fluorescence quantum yield increased from 1.5 to 8 % after conjugation with electron-rich hexadecylamine (HDA) to organic dye Cy7. The photostability of the nanoprobe GCF-HDA was dramatically improved after involving the newly synthesized dye. Molecular dynamics simulationdemonstrated that the GCF-HDA is composed of 2.0-3.5 nm clusters and in each cluster the head groups of the amphiphilic molecules assemble together and the tail groups point outwards. The r1 and r2 relaxivities of GCF-HDA were found to be 11.87 and 19.91 $mM^{-1}s^{-1}$ per Gd(III) chelate at 0.5T, respectively. *In vitro* cellular imaging with human glioma U-87 MG cells showed that the GCF-HDA was able to enter the cells and accumulate in the cytoplasm. The targeted GCF-HDA resulted in higher MR contrast enhancement and stronger fluorescence intensity than the corresponding non-targeted probe GC-HDA in the tumor tissue 96 hours post injection. *Ex vivo* fluorescence imaging and histological analysis of the tumor tissue further confirmed the specific binding ability of the GCF-HDA.

## 1. Introduction

Accurate detection and diagnosis are crucial aspects to consider in the successful treatment of cancer at an early stage. Recently, non-invasive imaging techniques for cancer diagnosis including optical imaging[1], magnetic resonance imaging(MRI)[2], X-ray computed tomography(CT)[3], positron emission tomography (PET)[4] and ultrasonic imaging[5] have led to rapid advances in our understanding of human anatomy and physiology. Among these modalities, MRI is able to non-invasively visualize deep tissue areas in the human body with high spatial resolution and is therefore a widely used imaging tool in clinical practice. However, the sensitivity of MRI in cancer diagnosis is constrained by the ubiquitous presence of protons (i.e. water) in virtually all tissue areas. Common amplification strategies involve the use of smart contrast agents. Near-infrared (NIR) fluorescence imaging, an excellent complementary optical imaging method, has been established as a powerful imaging tool for *in vivo* molecular imaging of specific targets with high sensitivity. The combination of these two imaging modalities paves the way for utilizing a single bimodal probe to achieve high spatial resolution and high sensitivity in a simultaneous fashion, without the need for a radiation source.[6, 7] For instance, the organic NIR dye Cy5.5 attached to iron oxide nanoparticles cross-linked by dextran as a MRI/NIR bimodal nanoprobe (NP) has already been employed for the preoperative visualization of brain tumor with MRI and NIR imaging in an effort to discriminate tumorous from normal tissues.[8] In order to increase the sensitivity and accumulation behavior of the probe in tumor regions, the peptide Cltx that selectively targets glioma tumor, together with the NIR fluorescent dye Cy5.5 were conjugated by poly(ethylene glycol)(PEG) onto the surface of iron oxide nanoparticles for glioma tumor imaging.[9] A tumor targeting micelle based on a poly( ε -caprolactone)-b-poly(ethylene glycol) block copolymer (PCL-*b*-PEG) functionalized with diethylenetriamine pentaacetic acid-gadolinium (DTPA-$Gd^{3+}$) on the outer shell with $T_1$ contrast ability as well as a NIR dye present in the micelle core, has already been reported featuring high longitudinal relaxivity for bimodal tumor imaging.[10] Moreover, supramolecular conjugates like fluorescent paramagnetic bimodal liposomes have also been developed in an effort to enhance the cellular penetration ability of Gd-based agents into tumorous tissues for tumor imaging.[11-14]

[a] *Division of Biotechnology, Dalian Institute of Chemical Physics, Chinese Academy of Science, Dalian 116023, China. Fax & Tel: +86-411-84379139; E-mail: 2468750030@qq.com.*
[b] *University of the Chinese Academy of Science, Beijing 100049, China.*
[c] *National Engineering Research Center of Seafood, Liaoning Province Key Laboratory of Seafood Science and Technology, School of Food Science and Technology, Dalian Polytechnic University, Dalian 116034, China.*
[d] *Molecular Modeling and Design Group, State Key Laboratory of Molecular Reaction Dynamics, Dalian Institute of Chemical Physics, Chinese Academy of Science, Dalian 116023, China.*
† Footnotes relating to the title and/or authors should appear here. Electronic Supplementary Information (ESI) available: [details of any supplementary information available should be included here]. See DOI: 10.1039/x0xx00000x

This journal is © The Royal Society of Chemistry 20xx



Published on 05 October 2015. Downloaded by University of Rhode Island on 12/10/2015 04:19:23.

Journal of Materials Chemistry B Accepted Manuscript

Please do not adjust margins

View Article Online
DOI: 10.1039/C5TB01160D


Published on 05 October 2015. Downloaded by University of Rhode Island on 12/10/2015 04:19:23.

NIR dyes with large Stokes shift and MRI contrast agents with high relaxivity are highly desirable components for the development of a MRI/NIR bimodal probe. NIR organic dyes with unique absorption wavelengths in the range of 600-900 nm can result in deep tissue penetration for *in vivo* optical imaging due to the fact that in this range the tissue absorption is weak and the auto-fluorescence background is negligible.[15-17] However, the Stokes shift of the majority of NIR dyes like indocyanine green (ICG) used in clinical applications is less than 30 nm, leading to significant overlap of the excitation/emission spectra. This often causes considerable interferences in optical imaging, as well as fluorescence quenching.[18] Peng and co-workers reported the synthesis of a series of heptamethine cyanine dyes obtained through nucleophilic substitution reactions at the central position of Cy dyes to obtain a large Stokes shift (>140 nm) and higher quantum yield.[19] This finding could be useful for the production of more efficient MRI/NIR bimodal probes. On the other hand, small molecular paramagnetic contrast agents are often used in a clinical setting in order to improve the MRI contrast ratio by shortening the relaxation times of the water $^1$H NMR resonance.[20] Unfortunately, such contrast agents have been proved to be tissue nonspecific, extracellular compounds and their efficiency in molecular imaging has been limited due to their lower specificity and lower $r_1$ relaxivity. Supramolecular liposomes can not only provide greater and prolonged contrast enhancement at a generally lower dosage, but are also capable of carrying a large number of gadolinium chelates and targeting moieties. The results from MR angiography and tumor angiogenesis imaging suggest that supramolecular liposomes provide an optimal platform for the development of target-specific MRI/NIR bimodal contrast agents.[21, 22]

In this work, we report a method based on a simple hydrophobic/hydrophilic interaction mechanism for the preparation of a folate-receptor (FR) targeted MRI/NIR bimodal probe through self-assembly of small molecule amphiphilic liposomes. Notably, a novel heptamethine cyanine dye with large Stokes shift has been prepared as the NIR imaging moiety and an amphiphilic gadolinium(III) complex, namely DO3A-Gd$^{3+}$, serves as $T_1$ MR contrast agent. The prepared MRI/NIR bimodal probe proves to be of irregular spherical shape with a size less than 50 nm. Furthermore, the probe features excellent fluorescent and relaxation properties with good water solubility under physiological conditions. The formation mechanism of the self-assembled probe was studied using a Coarse-Grained (CG) model of a molecular dynamics (MD) simulation. The large Stokes shift of the NIR feature combines the characteristics of deep tissue penetration and a reduced overlap of the corresponding excitation/emission spectra in tissues, expected to significantly enhance the signal-to-noise ratio. Presumably, the bimodal probe presented in this work is able to combine the functions of FR targeted, NIR fluorescence and MR imaging into one nano-system. Its feasibility for both *in vitro* and *in vivo* imaging has also been investigated.

## 2. Materials and methods

### 2.1 Materials and Reagents

Hexadecylamine (HDA), folic acid (FA), dicyclohexylcarbodiimide(DCC) and N-hydroxysuccinimide(NHS) were purchased from Aladdin and Sigma-Aldrich (Shanghai, China). Tert-butyloxycarbonyl1,4,7,10tetraazacyclododecane-1,4,7,10-tetraacetic acid (DOTA) was purchased from Synpartner PharmTech Co., Ltd (Zhejiang, China). 2,3,3-trimethyl-indole and trifluoroaceticacid (TFA) were purchased from Zahn Chemical Inc. (Shanghai, China). Gadolinium acetate hydrate was purchased from Alfa Aesar Chemical Inc (Tianjin, China). Iodine propionate was purchased from Beijing J & K Technology Inc (Beijing, China). Column chromatography was performed using 200 to 400 mesh silica gel from Qingdao Ocean Chemical Inc (Qingdao, China).All the organic solvents were analytical grade, and used without further purification. Human glioma cells U-87 MG cells were purchased from American Type Culture Collection (ATCC). Female BALB/c-nu mice were purchased from the Animal Center of Dalian Medical University (Dalian, China).

### 2.2 Instrumentation and Characterization

All synthesized compounds were characterized by matrix-assisted laser desorption ionization time-of-light (MALDI-TOF) mass spectroscopy (5800, AB SCIEX) with α -cyano-4-hydroxycinnamic acid as a matrix. The UV-vis absorption spectra were recorded on a UV-2550 spectrophotometer (Shimadzu, Japan) and the NIR fluorescence emission spectra were measured by a fluorescence spectrophotometer system (LS-55, PerkinElmer, USA). The particle size distribution and stability were operated by the laser particle size analyzer and zeta potential analyzer. High-resolution transmission electron microscopy (HRTEM) observations were obtained with a JEM-2100 transmission electron microscope operating at 200KV. The samples for HRTEM were prepared by drying sample droplets from water dispersion onto a 230-mesh Cu grid coated with a lacey carbon film and negative stained by phosphotungstic acid. The contents of Gd element in the solution were measured by inductively coupled plasma-optical emission spectroscopy (ICP-OES 7300DV, PerkinElmer，JAP). The cells were imaged by confocal microscope system (FV1000MPE, Olympus, JAP). MRI experiments were conducted on a 0.5T magnet scanner (MiniMR-Rat, Shanghai Niumag Corporation, Shanghai, China). NIR experiments were performed on a maestro animal in vivo imaging system (MK50101-EX, CRI, USA). The histological sections were analyzed by confocal laser scanning microscope (Leica, TCS-SP2, Germany) with an inverted microscope (Leica, DMIRE2, Germany).

### 2.3 Synthesis of MRI lipid Gd-DOTA-HDA (1)

The MRI lipid Gd-DOTA-HDA was synthesized by three sections. Firstly, tert-butyloxycarbonyl DOTA acid (1.0026g, 1.75 mmol), DCC(1.8087g, 8.77mmol) and N-hydroxysuccinimide NHS(0.2448g, 2.13mmol) were added to a dry round-bottomed flask followed by the addition of $CH_2Cl_2$

Journal of Materials Chemistry B Accepted Manuscript


This journal is © The Royal Society of Chemistry 20xx

View Article Online
DOI: 10.1039/C5TB01160D


Published on 05 October 2015. Downloaded by University of Rhode Island on 12/10/2015 04:19:23.

(10 mL). The reaction was stirred at room temperature for 2 h to obtain active DOTA ester (compound **4**, Scheme S1, ESI). Then hexadecylamine (HDA) (0.5065g, 2.1mmol) and triethylamine ($Et_3N$) (732μL, 5.25mmol) were added into the mixture solution under room temperature with stable stirring for another 12 h. The solvents were removed by rotatory evaporation and the crude mixture was purified by adding appropriate volumes of diethyl ether. The precipitation was collected and dried under vacuum, yielding tert-Butyl-protected DOTA-HDA (compound **5**, Scheme S1, ESI) as a yellow powder. The compound **5** was dissolved in a 1:1 mixture of TFA/$CH_2Cl_2$ and stirred at room temperature for 2 h. The solution was concentrated by a rotavapor, and the mixture resuspended in petroleum ether and freeze-dried to yield a yellowish oil DOTA-HDA (**6**) (Scheme S1, ESI) (621mg, 57% yield). Finally, the compound**6** (621mg, 0.990mmol) was dissolved in 30 mL of deionized water in a round-bottom flask and pH value was adjusted to 5-6 with 0.1 M NaOH solution. A stoichiometric amount of $(CH_3COO)_3Gd.H_2O$ (0.3481 g, 0.988 mmol) was also added to the above solution and the reaction was stirred in a 90°C oil bath for 2 h. After freeze-drying, a buff powder was yield (523 mg, 68% yield). $R_f$ [$CH_2Cl_2$/MeOH/$H_2O$ 34.5:9:1 v/v] 0.23. No detectable free $Gd^{3+}$ was measured by the Xylenol orange test. MALDI TOF mass spectroscopy [(m/z, $[M+H]^+$):783.36(calculated), 783.5862(observed); (m/z, $[M+Na]^+$): 805.36 (calculated), 805.5742(observed)].

**2.4 Synthesis of NIR lipid Cy7-HDA (2)**

**Compound 7:**Phosphoryl chloride($POCl_3$ 10mL, 0.109 mol) was added drop wisely into a solution of DMF/DCM(20mL, 1:1,v/v) under stirring in ice/water bath, followed by adding cyclohexanone (2.63mL, 25.5mmol). The solution was then heated to 80°C and refluxed for 3 h. The mixture was transferred into a beaker and 100 mL of water was added under ice/water bath, yielding a solid yellow product. After collecting with filtration and washing with ice-cooled water, the compound **7** (Scheme S2, ESI) was dried under vacuum (1.459g, 33.3% yield).

**Compound 8:** To10 mL of toluene was added 2,3,3-trimethyl-indole (2.225g, 13.9mmol) and iodine acid (1.875g, 9.4mmol) and the solution was stirred and refluxed in a 100°C oil bath for 3 h. After adding 15mL of diethyl ether, the solvent was removed by vacuum evaporation, yielding a red solid product. The product was then dissolved and precipitated in a mixture of ether and acetone (1:1, v/v) for several times to yield compound **8** (Scheme S2, ESI) after lyophilization (2.204g, 65.3% yield).

**Compound 9:** Compound**7** (0.532g, 3.09 mmol) and compound **8** (2.204g, 6.14mmol) were added to the solvent of toluene (5mL) and DMF(12mL) and stirred in a 160°C oil bath for 10 h in dark. The solvent was removed by rotatory evaporation and the crude product was purified by precipitation in diethyl ether and water solution. After washing with ethanol, the NIR organic dye compound **9** (Scheme S2, ESI) was obtained (701.1mg, 31.4% yield).

**Compound 2** (Cy7-HDA)**:** HDA (2.333g, 9.669mmol) and compound **9** (0.7011g, 0.9655mmol) were added into DMF (15mL) and $Et_3N$ (673 μL, 4.8275mmol). The mixture was then heated to 70°C under stirring for 10h in dark. The solvent was then removed by rotatory evaporation, and the crude mixture was purified by flash column chromatography (eluted with ($CH_2Cl_2$/MeOH/$H_2O$ 40:20:1), v/v) to yield the compound **2** (Scheme S2, ESI) as a dark green powder (211mg, 23%yield). $R_f$ [$CH_2Cl_2$/MeOH/$H_2O$ 40:20:1 v/v] 0.6. The final product was characterized by MOLDI-TOF [(m/z, $[M-I]^+$): 804.57 (calculated), 804.6874(observed); (m/z, $[M-I+Na]^{2+}$): 827.57(calculated), 826.8386(observed)].

**2.5 Synthesis of FR-targeted lipid FA-HDA (Compound3)**

FR-targeted lipid FA-HDA (Compound **3**, Scheme S3, ESI) was synthesized in two steps. Firstly, the γ-COOH group of FA (1.0034g, 2.3mmol) was activated by DCC/NHS catalyst system (molar ratio of FA:DCC:NHS = 1.1:5.5:1.2) with $Et_3N$ (1.57mL, 11.3mmol) in anhydrous dimethyl sulfoxide (DMSO, 12 mL) under the continuous stirring for 12 h in the dark at room temperature. Secondly, HDA in 8 mL ethyl acetate was added dropwisely into the above solution and the reaction was allowed to proceed in the dark with stirring for 24 h. After removing the insoluble white precipitate, the solvent was removed through a rotary evaporator and the crude product was yielded by precipitating in diethyl ether and dried under vacuum (515.1mg, 37% yield). The final product was also characterized by MOLDI-TOF [(m/z, $[M+H]^+$): 665.7993(observed), [M]: 664.41(calculated)].

**2.6 Preparation of MRI/NIR bimodal probe**

With three functional amphiphilic molecules in hand, liposome NPs were prepared with defined molar ratios of each individual lipid. Targeted NPs consisted of Gd-DOTA-HDA/Cy7-HDA/FA-HDA (GCF-HDA) with a molar ratio of 5:5:1. Briefly, appropriate volume of Gd-DOTA-HDA and Cy7-HDA in methanol and FA-HDA in tetrahydrofuran (THF) were placed in a round-bottom flask and stirred to ensure totally mixing of the lipids. The solvents were removed slowly by a rotatory evaporator, then appropriate volume of ultra-pure water was added and the resulting solution was sonicated for 40 min to obtain NPs. Then, the solution was filtered using 0.8 μm Millipore filters to remove large particles and the final solution was stoked at 4°C. The size of the NPs was measured by dynamic light scattering (DLS). For in vivo experiment, the liposomes NPs were diluted by saline to obtain a 5 m$MGd^{3+}$solution. For non-targeted NPs preparation, the procedure was the same without adding FA-HDA molecules.

**2.7 Molecular dynamics (MD) simulation based on coarse-grained (CG) model**

The Gay-Berne electric multipole (GBEMP) parameters for the bond stretching, angle bending and torsional potentials were obtained by fitting to the atomistic profiles of the potentials of mean force (PMFs) constructed from atomic configurations (OPLS force field)[23] of liquid organics (Cy7-HDA, Gd-DOTA-HDA and FA-HDA). All bonded parameters are given in Supporting Information. The GBEMP MD simulation protocol used in this study is described as follows. The atomistic structure of each system was converted into its CG representation in Euler coordinates containing three Cartesian coordinates (x, y and z)

Journal of Materials Chemistry B Accepted Manuscript



Please do not adjust margins

View Article Online
DOI: 10.1039/C5TB01160D


Published on 05 October 2015. Downloaded by University of Rhode Island on 12/10/2015 04:19:23.

and three Euler angles (ϕ, θ and ψ) of the centers of mass. All GBEMP simulations were carried out in the Generalized Kirkwood (GK) implicit solvent [24] in the TINKER-based "GBEMP" program and the equation of motion was integrated using the Euler's rigid body integrator with an integration step of 10 fs. The non-bonded interaction cut off was set to 16 Å with a truncate scheme, and the Gay-Berne and electrostatic interactions of 1-2 and 1-3 neighbors were scaled with a factor of 0.003 and 1.0, respectively. Each nucleic acid system was minimized and subsequent runs were carried out under the temperature of 300 K for 6 -12 ns.

**2.8 MRI analysis of bimodal NPs**

Relaxation rate measurements of the bimodal NPs was carried out by using the stoke solution (targeted and non-targeted) diluted with water to obtain five different gadolinium concentration in the range of 0.0625-1.0 mM [Gd]. $T_1$ and $T_2$ relaxation time of each sample were measured with an inversion-recovery (IR) pulse sequence and a Carr-Purcell-Meiboom-Gill (CPMG) sequence, separately, using a 0.5T MRI system. The $r_1$ or $r_2$relaxation rate was defined as the slope of the line generated from a graph of 1/T ($1/T_1$ or $1/T_2$) vs the atomic concentration of Gd element (shown in equation 1). Additionally, the $T_1$-weighted axial images were acquired using the Spin Echo (SE) sequence. The parameters for relaxation rate analysis were SW = 200, RFD = 0.010 ms, TW = 7000 ms, RG1 = 20, DRG1 = 3, NS = 4, DL1 = 0.275, NECH = 10000. Parameters for MRI images were TR = 500 ms, TE = 19 ms, FOV = 100×100 $mm^2$, slices = 3, slices width = 2.5 mm, slice gap = 1.0 mm, average = 4, matrix size = 256×192.

$$C \times r + 1/T_w = 1/T_m \quad (1)$$

where r is the relaxivity rate; C is the Gd concentration values; $T_w$ and $T_m$ are relaxation time of the pure solvent and the aqueous solution containing bimodal NPs, respectively.

**2.9 In vitro fluorescent cell uptake assay and cytotoxicity assay**

Human glioma cells U-87 MG cells were cultured in high glucose Dulbecco's Modified Eagle Media (DMEM) (Gibco) medium containing 10% fatal bovine serum (FBS) (TransGen Biotech), 1% penicillin/streptomycin, in 35 mm culture dishes ($2\times10^4$ cells per well, 1ml of DMEM medium) at 37°C under 5% $CO_2$. The cells were grown until 80% confluent and 1 mL of targeted and non-targeted probe (1 mM[Gd]/L) was added, respectively. After incubation under 5% $CO_2$ atmosphere at 37 °C for 2 or 4 h, the cells were washed with PBS (pH-7.4) for three times to remove the extra probes and imaged by confocal microscope system equipped with an external 633 nm excitation laser.

The cytotoxicity of the GCF-HDA was evaluated by Cell Counting Kit-8 (CCK-8) viability assay. U-87 MG cells were seeded in to a 96-well plate with a density of $1\times10^4$ per well and cultured in the same way mentioned above for 24 h. The medium was replaced with fresh medium containing GCF-HDA nanoprobe at different concentrations ($1\times10^{-6}$-0.1mM [Gd]). After incubating for 6 and 12 h, the medium was removed and the cells were washed with PBS for three times. Then 150 μL of CCK-8 (10% in fresh medium) solution was added into the cells and incubated for another 1 h. 100 μL supernatant was transferred to a 96-well plate and the absorbance values at a wavelength of 450 nm in each well were measured using a Synergy H1 hybrid reader (BioTek Instruments, Inc, USA).

**2.10 *In vivo* MRI and NIR study**

Female BALB/c-nu mice (5-6 weeks) were purchased from the Animal Center of Dalian Medical University. $2\times10^6$ U-87 MG cells in PBS/Matrigel mixture (1:1 v/v) were inoculated into the right flank of the nude mice. When the tumors reached 0.3-0.5 cm in diameter, the mice were randomly divided into groups with four mice for each group. The bimodal probes tumor-targeted GCF-HDA or non-targeted GC-HDA saline solution were injected from tail vein at a dose of 0.05 mmol-Gd/kg. The mice were anesthetized with 2% isoflurane and scanned with a 0.5T permanent magnet MRI scanner at pre-injection and at 24, 48, 72, 96, 120 and 144 h post-injection using a SE sequence with the parameters TR=500ms, TE=19ms, FOV=100 × $100mm^2$, slices=12, slices width=1.8mm, slice gap=0.5mm, average=4, matrix size=256×192. In vivo contrast enhancement of MRI images was analyzed using Osirix software. A region of interest was drawn around the whole tumor and the mean signal intensity was captured as a directly reflection of the longitudinal relaxation time at each time point. Following MRI imaging at each time point, the spectral NIR images were acquired by a Cri maestro EX *in vivo* imaging system using the appropriate filter for probe (excitation: 605 nm; emission: 645 nm long-pass filter; 10 nm steps).Exposure times were automatically calculated and kept the same for GCF-HDA and GC-HDA NPs. Statistical analysis was performed using a one-tailed Student's t-test, assuming statistical significance at $p < 0.05$.

**2.11 *Ex vivo* NIR imaging and histological analyses.**

After MRI and NIR imaging at 96 h, the mice were sacrificed and tumor tissue and main organs were isolated for *ex vivo* NIR imaging with CRi maestro imaging system. Then the tumor tissues were cryosectioned into 6-μm slices and imaged immediately at 20X on a confocal laser scanning microscope equipped with 633 nm leaser source. The images were processed with the Olympus FV software.

## 3. Results and discussion

**3.1. Synthesis and characterization**

Tumor targeted bimodal MRI/NIR liposome GCF-HDA NPs have been synthesized with three kinds of amphiphilic molecules through self-assembly in aqueous solution using an ultrasonicator (Scheme 1). Gd-DOTA-HDA (compound **1**) was prepared via the amphiphilic species DOTA-HDA (compound **5**) from the amidation of DOTA-NHS (compound **4**) with HDA. The tert-butyloxycarbonyl group on DOTA-HDA has been removed by TFA to obtain compound **6** with high yield and purity. Afterwards, the DOTA-HDA was complexed with gadolinium(III) acetate hydrate at pH = 5-6 in aqueous solution at 90 °C for 2 hours to obtain the paramagnetic, amphiphilic compound Gd-DOTA-HDA **1** (Scheme S1, ESI). As shown in Fig.S2, the absorbance of dialyzate is similar to that of the PBS

Journal of Materials Chemistry B Accepted Manuscript


This journal is © The Royal Society of Chemistry 20xx

View Article Online
DOI: 10.1039/C5TB01160D


Published on 05 October 2015. Downloaded by University of Rhode Island on 12/10/2015 04:19:23.

control. However, the absorbance of Gd-DOTA-HDA and free $Gd^{3+}$ (5 mM) was 1.51 and 2.32-fold as compared with that of the dialyzate. This result strongly suggested that the Gd-DOTA-HDA was sable in PBS for storage as long as 7 days.

The NIR organic dye Cy7-HDA (compound **2**) was synthesized by reacting intermediate **7** with intermediate **8** at high temperature followed by conjugation of HDA as an electron-donating moiety at the central position of Cy7 dye to obtain the NIR amphiphilic molecule (compound 2) (Fig. 1a and Scheme S3, ESI)**.** The NIR dye, heptamethine cyanine (Cy7), has already been extensively used in tumor imaging and cancer therapy in recent years, mostly due to their thermal-stability and photo-stability.[25-27] However, this NIR dye still exhibits a significant overlap of the excitation/emission spectra due to a small Stokes shift (< 30 nm) (Fig. 1b)**.** After conjugation with electron-rich HDA, the Stokes shift of Cy7-HDA increased to 150 nm, which represents a 5-fold increase compared to that of Cy7. This significant change might be attributed to the intra-molecular charge transfer (ICT) between the charge donor HDA and the acceptor, the Cy7 dye.[19] The fluorescence quantum yield of Cy7 was found to be 1.5% and increases to 8% after formation of Cy7-HDA by using ICG as a reference (Table 1). The latter property is of great advantage for *in vivo* tumor imaging. Finally, the FR-targeted amphiphilic molecules FA-HDA were synthesized via amide coupling reaction of HDA with the DCC/NHS activated FA ester (Scheme S4, ESI). All of the intermediates and final compounds have been characterized by MOLDI-TOF mass spectrometry (Fig. S1, S3-4, ESI).

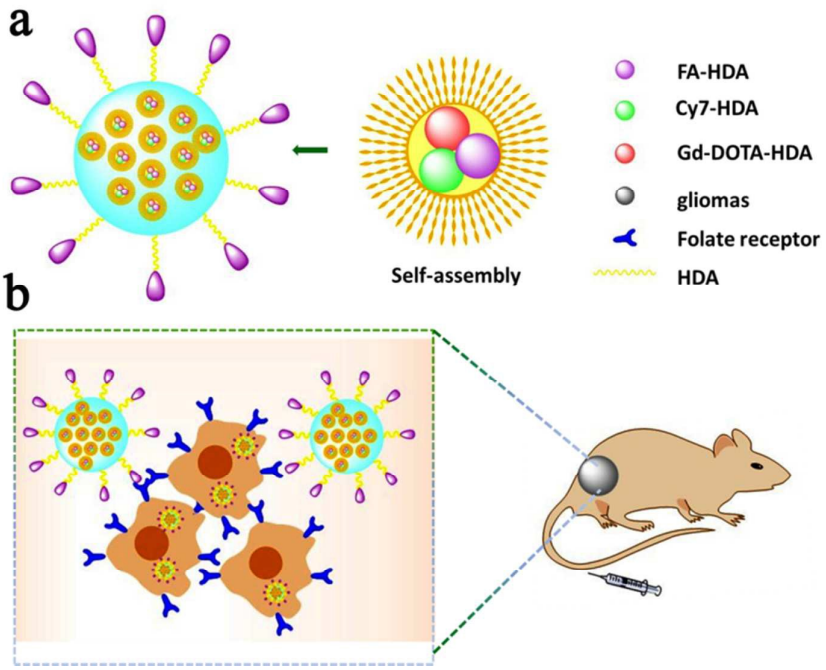


**Scheme 1.**(a) Design of the tumor-targeted bimodal GCF-HDA NPs. (b) Schematic diagram of the GCF-HDA NPs as the targeted MRI/NIR bimodal probe for FR-mediated endocytosis, enabling MRI and NIR imaging of the glioma.

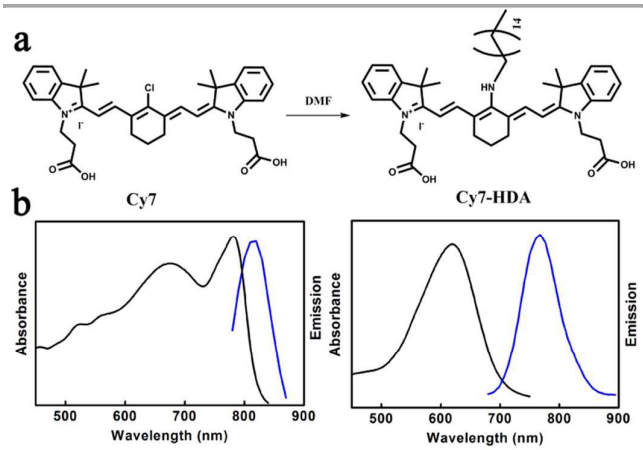


Fig.1. (a) Synthetic scheme for the amphiphilic heptamethine cyanine dyes. (b) Absorption (black) and emission (blue) spectra of dyes in ethanol (left for Cy7,ex735nm; right for Cy7-HDA,ex605nm).

**Table 1.**Photophysical characteristics of NIR dyes in ethanol.

| dye | Absorption $\lambda_{ab}$(nm) | Emission $\lambda_{em}$(nm) | Stokes shift(nm) | QY (%) |
|---|---|---|---|---|
| Cy7 | 780 | 810 | 30 | 1.5 |
| Cy7-HDA | 620 | 770 | 150 | 8.0 |

A bimodal MRI/NIR liposome NP has been constructed through a self-assembly process of the above mentioned three kinds of functional amphiphilic molecules, Gd-DOTA-HDA, Cy7-HDA and FA-HDA (GCF), at a molar ratio of 5:5:1 in aqueous solution upon ultrasonication. The non-targeted liposomes were also prepared as a control in this study with a molar ratio of Gd-DOTA-HDA/Cy7-HDA determined to be 1:1. Upon combination

Journal of Materials Chemistry B Accepted Manuscript



Please do not adjust margins

View Article Online
DOI: 10.1039/C5TB01160D


Published on 05 October 2015. Downloaded by University of Rhode Island on 12/10/2015 04:19:23.

of the three functional groups through self-assembly, the absorption spectrum of GCF nanoparticles is shown in Fig. S5 (ESI), which exhibits the presence of three kinds of functional amphiphilic molecules, Gd-DOTA-HDA, Cy7-HDA and FA-HDA. The liposomes have been characterized by HRTEM imaging (Fig. 2a). It was observed that the liposomes are of irregular spherical shape with a diameter ranging between 20 and 40 nm (Fig. 2b).Furthermore, some inlayed black spots could be found with a size of 1.8-3.5 nm (Fig. 2b, inset). The assembly process of the liposomes was assessed by molecular dynamics (MD) simulations based on a coarse-grained (CG) model (detailed information please see ESI). The initial structure (t = 0 ns) of the system consists of a bilayer (Fig. 2c) as well as a random assembly (Fig. S6, ESI). The potential energies have been monitored during GBEMP simulations of the two systems (bilayer and a random assembly). For each system, the energy landscape became flat after simulation for 9 ns, indicating that these systems reach their corresponding equilibria. GBEMP mapping for three self-assembly units is depicted in Fig. S7 (ESI). The CG model of Cy7-HDA (C) is composed of one elliptic rigid body and three disk-like rigid bodies, that of Gd-DOTA-HDA (D) is made up of four elliptic rigid bodies and that of FA-HDA (F) consists of one elliptic rigid body and one disk-like rigid body. The hydrophobic tail of each model is represented by one elliptic rigid body that contains one Gay-Berne site and one non-interacting EMP site. The equilibrium conformation of the mixture, independent of its starting conformation, shows similar characteristics: (1) the whole system (C:D:F=5:5:1) is composed of clusters with various sizes (2.0~3.5 nm in diameter); (2) in each cluster the head groups of the amphiphilic molecules assemble together and the tail groups point outwards. The non-interacting EMP site (denoted by orange filled circle) would not involve in electrostatic interaction but serve just as the connection purpose. In each model, the corresponding CG particles of hydrophilic head group contain one Gay-Berne site and one EMP site which both share a same location shown by a red filled circle. In addition, one or two non-interacting EMP sites are included into each CG particle in order to connect two different rigid bodies. The effective energy function of GBEMP model was calculated as depicted in the section of GBEMP energy function (please see ESI). In this work, the bond stretching, angle bending and torsional potentials were parametrized by fitting to the atomistic profiles of the potentials of mean force (PMFs) constructed from atomistic conformations of self-assembly units (Fig. S8, ESI). To parametrize the Gay-Berne potentials for nucleic acid models shown in Fig. S7 (ESI), the atomistic energy profiles using OPLS atomistic force field in this study were constructed for the intermolecular van der Waals (VDW) interactions between two identical molecular fragments (homodimer), illustrated in Fig. S9 (ESI). In each case, diverse configurations were generated with different orientations (such as, cross, end-to-end, face-to-face, etc.) as well as at various separations. The initial Gay-Berne parameters for CG particles were derived through fitting to the corresponding atomistic energy profiles in gas phase using a generic algorithm. GBEMP force field for self-assembly units was listed in the Supporting Information (ESI). Through combination of the simulation results it was revealed that the blackspots in HRTEM images might be the clusters formed due to van der Waals (VDW) interactions of adjacent NPs. Similar structures have been reported previously involving self-assembled materials with small molecule amphiphilic compounds, which have also been studied in detail as potential candidates for drug delivery systems with controlled release properties.[28, 29]

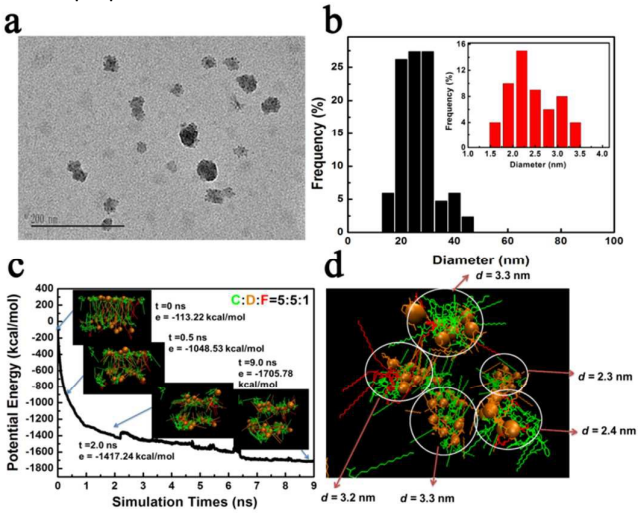


Fig.2.a) HRTEM images (negative stained by phosphotungstic acid) and b) size-distribution of GCF-HDA (black histogram) and the clusters (red histogram). c) Potential energies of the system (the mixture of C, D and F was built in a ratio of 5:5:1) evolving with MD simulation time. The starting structure (t = 0 ns) of the system was constructed as a form of bilayer. d) The final structure (t = 9 ns) of the system was obtained from the end of the GBEMP simulation. The three self-assembly units C, D and F are represented by green, orange and red lines respectively. Gd3+ ion is illustrated as a van der Waals (VDW) surface. The diameter (d) of each cluster is given in the plot.

In an effort to investigate the photostability of GCF-HDA NPs, the absorption spectra of GCF-HDA NPs in solution have been measured at different time points and compared with that of the ICG solution as control. As shown in Fig. 3a, the absorbance of the GCF-HDA NPs solution proved to be almost the same with light exposure for 24 hours, whereas that of the ICG solution degraded to 40% with the same exposure time (cf. Fig. 3b). The results obtained confirm that the newly synthesized Cy7-HDA shows a higher stability than ICG, which proves to be an important feature for applications in which a long time signal requisition and high tolerance to radiation are required, e.g. in near-infrared dyes used in bio-imaging. Furthermore, the stability of the hydrodynamic diameters of the liposome NPs in aqueous solution was also assessed. No significant change in the hydrodynamic particle size has been observed and the poly dispersity index (PDI) was found to be less than 0.3 over 6 days (Fig. 3c). The hydrodynamic diameter was in the range of 70-90 nm, which is larger than those obtained by TEM. This probably due to the aggregation of partial nanoparticles, which contribute great to total particle size in DLS analysis. It is necessary to mention that by TEM we image single particles, while DLS gives an average size estimation, which is biased toward the larger-size end of the

Journal of Materials Chemistry B Accepted Manuscript


This journal is © The Royal Society of Chemistry 20xx

Please do not adjust margins

View Article Online
DOI: 10.1039/C5TB01160D



Published on 05 October 2015. Downloaded by University of Rhode Island on 12/10/2015 04:19:23.

population distribution. The zeta potential measurements indicated that the GCF-HDA liposome NPs prove to be positively charged with a potential of 65.5 mV. Fig. 3d illustrates concentration-dependent $T_1$ weighted images of GCF-HDA and GC-HDA agents, wherein the GCF-HDA exhibits a better contrast enhancement. The $r_1$ and $r_2$ relaxivities of the liposome NPs have also been measured as shown in Fig. 3e and 3f. The $r_1$ and $r_2$ relaxivities of GCF-HDA were found to be 11.87 and 19.91 $mM^{-1}s^{-1}$ per Gd(III) chelate at 0.5T, with 9.27 and 15.53 $mM^{-1}s^{-1}$ per Gd(III) chelate for the control agent GC-HDA, respectively. The $r_1$ relaxivity of GCF-HDA was slightly higher than that of the corresponding non-targeted GC-HDA, but much higher than that of the clinically approved $T_1$ weighted contrast agent, Gd-DOTA (3.66 $mM^{-1}\cdot s^{-1}$).[20]

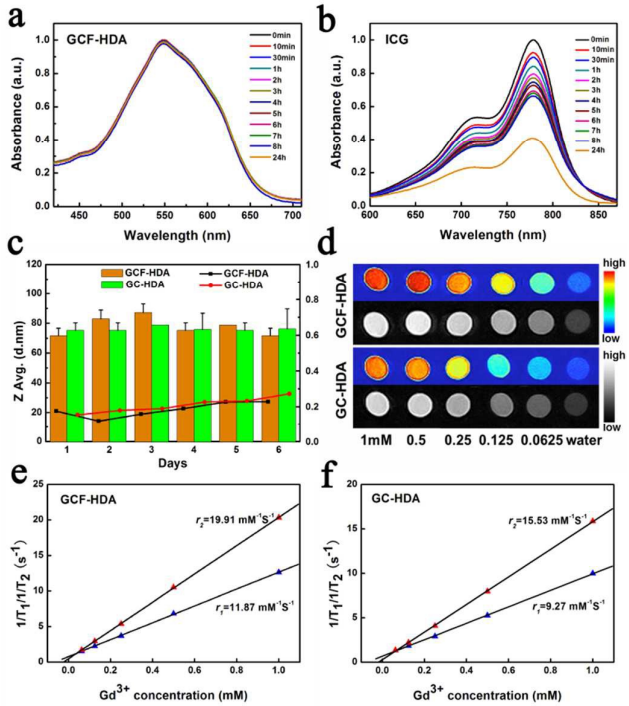


Fig. 3. Absorbance intensity change of GCF-HDA NPs (a) and ICG (b) over time when the solutions were exposed to ambient light. c) Monitoring the stability of the targeted and non-targeted nanoparticle solution at room temperature for 6 days. d) $T_1$-weighted images of the targeted and non-targeted groups. Plots of $1/T_1$ ($r_1$) and $1/T_2$ ($r_2$) versus the concentration of the Gd3+ element for the targeted group (e) and non-targeted group (f).

### 3.2 In vitro NIR fluorescence imaging and cytotoxicity

The selective targeting ability of GCF-HDA NPs for FR-expressing cells was evaluated by FR-positive human glioma U-87 MG cells via *in vitro* imaging. As shown in Fig. 4a, the liposomes were able to enter the cells and accumulate in the cytoplasm. The latter has been validated by the strong fluorescence intensity around the perinuclear region. The cell morphology remains intact, indicating that the cells feature a normal physiological activity in the presence of NPs. Notably, only U-87 MG cells treated with GCF-HDA NPs show greater fluorescence at 2 and 4 hours, respectively. This finding may be due to the active FR-mediated endocytosis that occurs on the surface of the cell membrane.[18, 30,31] FA is a vitamin, essential for the proliferation and maintenance of all cells.[30] On the membrane of a majority of malignant tumor cells, FR is often found to be over-expressed in order to capture any FA present in the serum as efficient as possible.[30] This is done to satisfy the uncontrolled proliferation needs of tumor cells. Considering the high affinity of tumor cells to FA via over-expressed FR, FA may be applied as a tumor-targeted media in FA-targeting cancer imaging and therapy.[32-34] The results obtained show that the GCF-HDA NPs can serve as a fluorescence probe for FR-positive tumor cell imaging. The viability of cells incubated with different concentrations of GCF-HDA NPs was shown in Fig. 4b. We can see that the GCF-HDA NPs displayed low toxicity (ca. 90%) to U-87 MG cells when the concentration of probes less than 0.01 mM [Gd] for 6 and 12 h.

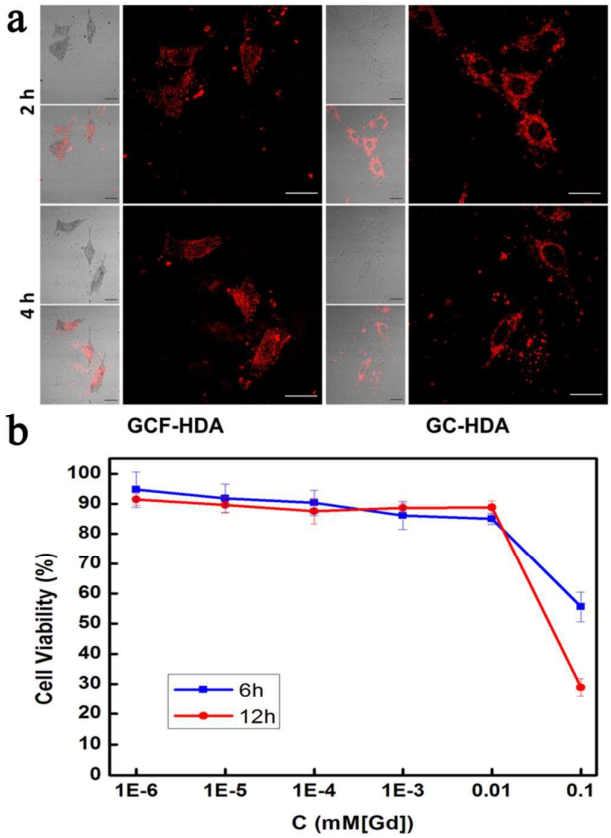


Fig. 4. a) The in vitro cellular uptake and cancerous cell imaging of bimodal NPs. Confocal microscope images with the 633 nm excitation wavelength both for FR-targeted and non-targeted NPs (1 mM [Gd]/mL) after incubation for 2 and 4 h (Scale bar represents 20 μm ). b) CCK-8 assay of U-87 MG cell viability after treatment with GCF-HDA NPs at the concentration of $10^{-6}$ – 0.1 mM [Gd] for 6 and 12 h. Cells treated with fresh medium were used as control.

### 3.3 *In vivo* MR/NIR tumor imaging

Tumor imaging is a valuable tool in the diagnosis and treatment of various tumor types, providing visual anatomical and physiological information noninvasively using appropriate probes. The $T_1$-weighted 2D MR images of tumor bearing mice contrast enhanced with the FR-targeted GCF-HDA and non-

Journal of Materials Chemistry B Accepted Manuscript



Please do not adjust margins

View Article Online
DOI: 10.1039/C5TB01160D


Published on 05 October 2015. Downloaded by University of Rhode Island on 12/10/2015 04:19:23.

targeted GC-HDA before and after tail vein injection are shown in Fig. 5a using a U-87 MG xenograft model (0.05 mmol-Gd/kg body weight, calculated for $Gd^{3+}$). The contrast gets gradually stronger over time as a result of bimodal probe accumulation in the tumor sites, reaching a maximum at 96 (GCF-HDA) or 72 hours (GC-HDA) post-injection. The images become darker over time after 96 hours of administration due to elimination and excretion of the agents. The quantitative MR enhancement in tumor regions before and after injection of the liposome bimodal probes is plotted in Fig. 5b. Administration of the targeted GCF-HDA resulted in higher MR contrast enhancement than that of the corresponding non-targeted probe GC-HDA in the tumor tissue at 96 hours ($p < 0.01$). This finding is likely due to the GCF-HDA with the FA moiety targeting the tumor tissue more readily than the non-targeted GC-HDA agent without FA. The FA functionalized liposomes can accumulate in tumor cells through receptor-mediated endocytosis at both high concentration and specificity. The vasculature in the solid tumor is often found to be vastly abnormal, resulting large gaps of 300-800 nm between adjacent endothelial cells.[30] This feature is the reason why NPs are able to accumulate in solid tumors efficiently. Therefore, the FA-targeting GCF-HDA exhibits a more rapid accumulation into the tumor sites through synergistic effects of enhanced permeability and retention (EPR) effect and FR-mediated endocytosis. On the other hand, the elimination rate of the targeted GCF-HDA was found to be slower than that of the non-targeted analogue GC-HDA, most likely due to the FA functionalization that increases the retention time of the NPs in tumorous tissues.[30]

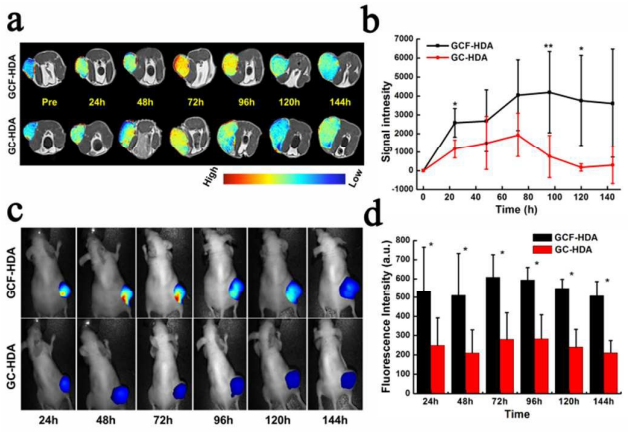


Fig.5. In vivo MRI/NIR images of U-87MG-bearing mice. a) MRI images (pseudocolor maps represent tumor area) were obtained at different intervals after tail vein injection of targeted GCF-HDA and non-targeted GC-HDA NPs, respectively, at 24, 48, 72, 96, 120 and 144 h. b) A quantification and statistical analysis of MRI signal intensity at the tumor region both for targeted and non-targeted group. c) NIR images acquired at 24, 48, 72, 96, 120 and 144h after tail vein injection of targeted GCF-HDA and non-targeted GC-HDA NPs, respectively. d) A quantification and statistical analysis of fluorescence intensity at the tumor region both for targeted GCF-HDA and non-targeted GC-HDA group. The data were represented as mean ±SD (n=4, *p<0.05, **p<0.01).

Fig. 5c shows the fluorescence images of the tumor bearing mice after tail vein injection of the targeted GCF-HDA and non-targeted GC-HDA at time points of 24, 48, 72, 96, 120 and 144 hours, respectively. A greater and more prolonged NIR fluorescence signal was observed in the tumor area using GCF-HDA compared to GC-HDA for at least 96 hours post-injection, indicating an effective binding of the targeting agent in the tumor tissue. Fig. 5d illustrates the statistical analysis of the fluorescence intensity in the tumor region at each time point. Remarkably, the fluorescence intensity of the FR-targeted GCF-HDA was stronger than that of GC-HDA, indicating that a larger amount of the probe accumulated in the tumor site. The latter finding is also consistent with the MR images obtained. Since the fluorescence NIR images obtained at the same time point followed MRI imaging, the quantitative fluorescence intensity (Fig. 5d) indicates a similar profile to that of MR imaging (Fig. 5b), further suggesting that the GCF-HDA accumulate in the tumor at 24 hours and increased progressively up to 96 hours post-injection. In our previously reported study with FA modified chitosan probes, we demonstrated that by using the targeting agents, a strong and prolonged tumor enhancement was observed with significant and localized accumulation in tumor tissues *in vivo*.[35]

### 3.4 Stability of the GCF-HAD in fetal bovine serum (FBS) solution.

The stability of the liposome NPs in the organism is important for bioimaging. The liposome GCF-HAD NPs were added into 50% fetal bovine serum (FBS) solution and their aggregation behavior was observed by DLS for 0 h, 0.5 h, 1 h and 24 h. The result in Fig. S10 showed that there was no aggregation, and the size distribution did not change much within 1 h. Even at 24 h, the liposome NPs showed a particle behavior with an increased size distribution. On the other hand, the intensity change of MRI and NIR was always in consistent with each other during the process of in vivo imaging. If they disentangled in the organism, they would be metabolic in their own way and the intensity change of MRI and NIR would become different. So the GCF-HAD NPs were stable in the organism after injection.

### 3.5 *Ex vivo* fluorescence imaging and histological analysis

*Ex vivo* fluorescence imaging and histological studies of the tumor tissue and major organs may provide further organ and structural information of FA binding on a microscopic level through fluorescence signal analysis. The *ex vivo* fluorescence images of tumors and major organs collected after 96 hours recorded on a Maestro EX *in vivo* imaging system are shown in Fig. 6a. A strong red fluorescence of Cy7-HDA was observed in the tumor regions of the mice injected with FR-targeted GCF-HDA, whereas an insignificant fluorescence signal was observed in the tumor tissue in the mice injected with non-targeted GC-HDA. Furthermore, NPs were found to accumulate in the liver and spleen as well with a negligible signal observed from the heart, lungs and kidneys. The quantitative fluorescence intensity profile shown in Fig. 6b illustrates that administration of FR-targeted GC-HDA NPs results in approximately a 5-fold increase in the fluorescence signal compared to GC-HDA at 96 hours. The histological analysis of the tumor tissue indicates that stronger red fluorescence was associated with the injection of FR-targeted GCF-HDA and an insignificant fluorescence signal was obtained from the tissue section in the mice injected with non-targeted

Journal of Materials Chemistry B Accepted Manuscript


This journal is © The Royal Society of Chemistry 20xx

Please do not adjust margins

View Article Online
DOI: 10.1039/C5TB01160D



GC-HDA (Fig. 6c). This result provides further evidence for the hypothesis that the targeting agent GCF-HDA exhibits a specific binding ability to the cells in the tumor tissue.

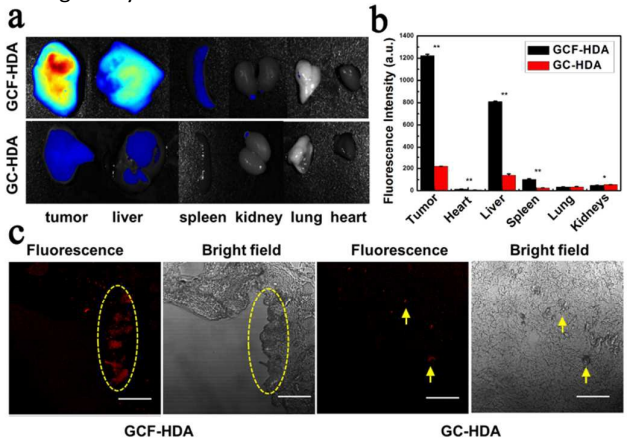


Fig. 6. a) *Ex vivo* NIR fluorescence images of tumors and major organs excised from the U87-MG bearing mice at 96 h post-injection of targeted GCF-HDA and non-targeted GC-HDA NPs, respectively. b) The fluorescence intensity quantification of the dissected tumors and major organs. c) NIR fluorescence and color images of frozen sections of tumor tissues. Circles point the area where the fluorescence signal of the targeted GCF-HDA come from, while the arrows show the sites where the relatively weak fluorescence signal of the non-targeted GC-HDA produce (Scale bar represents 150 μm). The data were represented as mean ± SD (n=3, *p<0.05, **p<0.01).

## 4. Conclusion

In summary, we have demonstrated a simple, yet rapid synthetic method for the production of a novel water-soluble bimodal MRI/NIR liposome nanoprobe for *in vitro* cellular imaging as well as *in vivo* MRI and NIR tumor molecular imaging. The bimodal probe has been prepared by self-assembly of three kinds of amphiphiles in aqueous solution. Excellent fluorescence characteristics have been obtained after structural incorporation of a heptamethine cyanine Cy7 derivative. Furthermore, the formation mechanism of the assembly process has also been explored through MD simulations. Through functionalization with the targeting agent FA, we have demonstrated the effectiveness of the bimodal liposomes to actively target tumor cells via *in vitro* cell imaging and via *in vivo* tumor imaging both through MRI and NIR imaging.

## Statements

The authors state that all animal studies were carried out at Specific Pathogen Free Animal Center at the Dalian Medical University according to the animal protocols (No. L2014014) approved by the Animal Ethics Committee (AEC).

## Acknowledgements

This work was financially supported by the National Nature Science Foundation of China (91227126), National Key Scientific Instrument and Equipment Development Project of China (2013YQ17046307) and the Nature Science Foundation of Liaoning Province, China (2013020177).

## References

1 E. Hemmer, N. Venkatachalam, H. Hyodo, A. Hattori, Y. Ebina, H. Kishimoto and K. Soga, *Nanoscale*, 2013, **5**, 11339-11361.
2 F. Zhang, X. Huang, L. Zhu, N. Guo, G. Niu, M. Swierczewska, S. Lee, H. Xu, A. Y. Wang, K. A. Mohamedali, M. G. Rosenblum, G. Lu and X. Chen, *Biomaterials*, 2012, **33**, 5414-5422.
3 S. Wen, K. Li, H. Cai, Q. Chen, M. Shen, Y. Huang, C. Peng, W. Hou, M. Zhu, G. Zhang and X. Shi, *Biomaterials*, 2013, **34**, 1570-1580.
4 Q. Liu, M. Chen, Y. Sun, G. Chen, T. Yang, Y. Gao, X. Zhang and F. Li, *Biomaterials*, 2011, **32**, 8243-8253.
5 H. Pan, N. P. Wu, H. Ding, Q. Ding, J. C. Dai, L. J. Ling, L. Chen, X. M. Zha, X. A. Liu, W. B. Zhou and S. Wang, *Plos One*, 2013, **8**, e74028.
6 L. C. Mimun, G. Ajithkumar, M. Pokhrel, B. G. Yust, Z. G. Elliott, F. Pedraza, A. Dhanale, L. Tang, A.-L. Lin, V. P. Dravid and D. K. Sardar, *J Mater Chem B*, 2013, **1**, 5702-5710.
7 X. F. Qiao, J. C. Zhou, J. W. Xiao, Y. F. Wang, L. D. Sun and C. H. Yan, *Nanoscale*, 2012, **4**, 4611-4623.
8 F. K. Moritz, M. Umar, S. K. Raymond, W. Ralph and J. Lee, *Cancer Res*, 2003, **63**, 8122-8125.
9 Veiseh O, Sun C, Gunn J, Kohler N, Gabikian P, Lee D, Bhattarai N, Ellenbogen R, Sze R, Hallahan A, Olson J and M. Zhang, *Nano Letters*, 2005, **5**, 1003-1008.
10 X. M. Sun, J. X. Xu, J. B. Tang, M. H. Sui and Y. Q. Shen, *Chinese J Polym Sci*, 2011, **29**, 427-430.
11 N. Kamaly, T. Kalber, A. Ahmad, M. H. Oliver, P. W. So, A. H. Herlihy, J. D. Bell, M. R. Jorgensen and A. D. Miller, *Bioconjugate Chem*, 2008, **19**, 118-129.
12 N. Ding, Y. Lu, R. J. Lee, C. Yang, L. Huang, J. Liu and G. Xiang, *Int J Nanomed*, 2011, **6**, 2513-2520.
13 N. Kamaly, T. Kalber, G. Kenny, J. Bell, M. Jorgensen and A. Miller, *Org Biomol Chem*, 2010, **8**, 201-211.
14 K. J. Chen, S. M. Wolahan, H. Wang, C. H. Hsu, H. W. Chang, A. Durazo, L. P. Hwang, M. A. Garcia, Z. K. Jiang, L. Wu, Y. Y. Lin and H. R. Tseng, *Biomaterials*, 2011, **32**, 2160-2165.
15 Y. Wang, T. Liu, E. Zhang, S. Luo, X. Tan and C. Shi, *Biomaterials*, 2014, **35**, 4116-4124.
16 C. Zhang, T. Liu, Y. Su, S. Luo, Y. Zhu, X. Tan, S. Fan, L. Zhang, Y. Zhou, T. Cheng and C. Shi, *Biomaterials*, 2010, **31**, 6612-6617.
17 Z. Guo, S. Park, J. Yoon and I. Shin, *Chem Soc Rev*, 2014, **43**, 16-29.
18 X. Zheng, D. Xing, F. Zhou, B. Wu and W. R. Chen, *Mol Pharm*, 2011, **8**, 447-456.
19 X. J. Peng, F. L. Song, E. H. Lu, Y. N. Wang, W. Zhou, J. L. Fan and Y. L. Gao, *J Am Chem Soc*, 2005, **127**, 4170-4171.
20 T. L. Kalber, N. Kamaly, S. A. Higham, J. A. Pugh, J. Bunch, C. W. McLeod, A. D. Miller and J. D. Bell, *Bioconjugate Chem*, 2011, **22**, 879-886.
21 T. Nakamura, K. Kawano, K. Shiraishi, M. Yokoyama and Y. Maitani, *Biol Pharm Bull*, 2014, **37**, 521-527.
22 N. Kamaly, T. Kalber, M. Thanou, J. D. Bell and A. D. Miller, *Bioconjugate Chem*, 2009, **20**, 648-655.
23 W. L. Jorgensen, D. S. Maxwell and J. Tirado-Rives, *J Am Chem Soc*, 1996, **118**, 11225-11236.
24 M. J. Schnieders and J. W. and Ponder, *J Chem Theory Comput*, 2007, **3**, 2083-2097.
25 L. Cheng, W. He, H. Gong, C. Wang, Q. Chen, Z. Cheng and Z. Liu, *Adv Funct Mater*, 2013, **23**, 5893-5902.

Published on 05 October 2015. Downloaded by University of Rhode Island on 12/10/2015 04:19:23.

Journal of Materials Chemistry B Accepted Manuscript



Please do not adjust margins

View Article Online
DOI: 10.1039/C5TB01160D


26 Q. Chen, C. Wang, Z. Zhan, W. He, Z. Cheng, Y. Li and Z. Liu, *Biomaterials*, 2014, **35**, 8206-8214.
27 Y. Yang, F. An, Z. Liu, X. Zhang, M. Zhou, W. Li, X. Hao, C. S. Lee and X. Zhang, *Biomaterials*, 2012, **33**, 7803-7809.
28 C. Fong, T. Le and C. J. Drummond, *Chem Soc Rev*, 2012, **41**, 1297-1322.
29 T. Kaasgaard and C. J. Drummond, *Phys Chem Chem Phys: PCCP*, 2006, **8**, 4957-4975.
30 W. Xia and P. S. Low, *J Med Chem*, 2010, **53**, 6811-6824.
31 Y. Cao and J. Yang, *Bioconjugate Chem*, 2014, **25**, 873-878.
32 H. Zhu, F. Liu, J. Guo, J. Xue, Z. Qian and Y. Gu, *Carbohyd Polym*, 2011, **86**, 1118-1129.
33 L. Li, Q. Yang, Z. Zhou, J. Zhong and Y. Huang, *Biomaterials*, 2014, **35**, 5171-5187.
34 C. Zheng, M. Zheng, P. Gong, D. Jia, P. Zhang, B. Shi, Z. Sheng, Y. Ma and L. Cai, *Biomaterials*, 2012, **33**, 5603-5609.
35 H. Wu, H. Zhao, X. Song, S. Li, X. Ma and M. Tan, *J Mater Chem B*, 2014, **2**, 5302.

Published on 05 October 2015. Downloaded by University of Rhode Island on 12/10/2015 04:19:23.

Journal of Materials Chemistry B Accepted Manuscript


This journal is © The Royal Society of Chemistry 20xx

View Article Online
DOI: 10.1039/C5TB01160D

Published on 05 October 2015. Downloaded by University of Rhode Island on 12/10/2015 04:19:23.

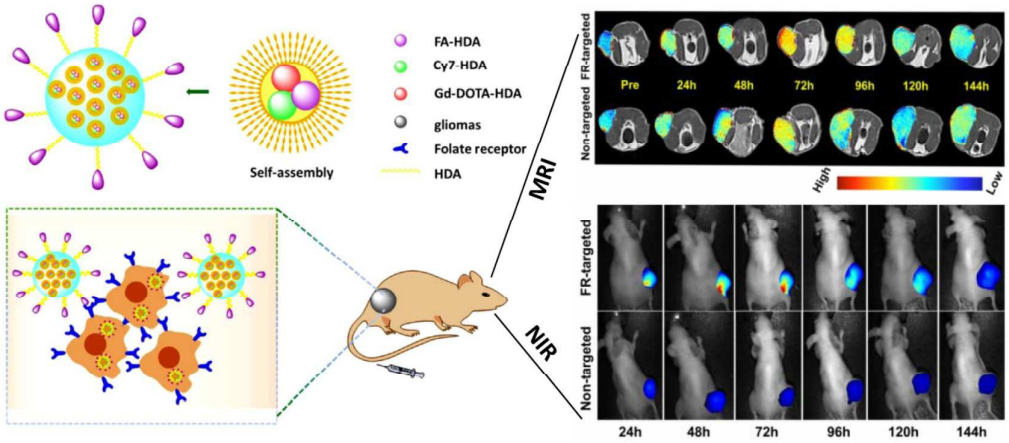


Journal of Materials Chemistry B Accepted Manuscript